

.....

## **Odour-plume dynamics influence the brain's olfactory code**

**Neil J. Vickers\*†, Thomas A. Christensen\*, Thomas C. Baker‡ & John G. Hildebrand\***

*\* Arizona Research Laboratories Division of Neurobiology, The University of Arizona, PO Box 210077, Tucson, Arizona 85721, USA*

*‡ Department of Entomology, Iowa State University, Ames, Iowa 50011, USA*

.....

The neural computations used to represent olfactory information in the brain have long been investigated<sup>1-3</sup>. Recent studies in the insect antennal lobe suggest that precise temporal and/or spatial patterns of activity underlie the recognition and discrimination of different odours<sup>3-7</sup>, and that these patterns may be strengthened by associative learning<sup>8,9</sup>. It remains unknown, however, whether these activity patterns persist when odour intensity varies rapidly and unpredictably, as often occurs in nature<sup>10,11</sup>. Here we show that with naturally intermittent odour stimulation, spike patterns recorded from moth antennal-lobe output neurons varied predictably with the fine-scale temporal dynamics and intensity of the odour. These data support the hypothesis that olfactory circuits compensate for contextual variations in the stimulus pattern with high temporal precision. The timing of output neuron activity is constantly modulated to reflect ongoing changes in stimulus intensity and dynamics that occur on a millisecond timescale.

In order to examine the relationship between the fine-scale structure of a natural odour plume and the complex patterns of odour-evoked activity in the brain, we used a well-characterized olfactory subsystem in male moths that is devoted to processing information about the female sex pheromone<sup>11-14</sup>. First, an electroantennogram (EAG) was used to monitor the spatiotemporal properties of a pheromone plume generated inside a laboratory wind tunnel (Fig. 1a). Surprisingly, the structure of the odour

† Present address: Department of Biology, University of Utah, Salt Lake City, Utah 84112, USA.

plume varied substantially at different sampling points separated by as little as 5 cm (Fig. 1b). At low wind speeds, both the largest EAG bursts and the most frequent fluctuations in EAG activity occurred in the central zone of the plume (Fig. 1c, centre), with virtually no activity at the peripheral sampling sites. As wind speed increased, however, the plume became more dispersed, with larger-amplitude EAG bursts occurring more frequently at the peripheral sites. Burst amplitude generally decreased as wind speed increased, and the location of the largest-amplitude responses shifted from the plume centre to the periphery (Fig. 1c). At the highest wind speed, the centre of the plume was characterized by higher-frequency, lower-amplitude bursts (Fig. 1c). Thus, in a natural airborne plume, odour contacts with the antennae are brief and frequent (up to  $5\text{ s}^{-1}$ ), and antennal responses furthermore show significant variation in amplitude over the course of stimulation (Fig. 1b and c). These intrinsic plume dynamics mean that very minor shifts in the position of a stationary antenna relative to the odour source resulted in large differences in the detected spatiotemporal pattern of odour striking the antenna.

To address the issue of how these spatiotemporal patterns might be further modified when an animal engages in typical locomotory activity (such as flight), male moths (*Heliothis virescens*) were fitted with a third antenna as an EAG monitor, and then allowed to fly upwind in a natural pheromone plume<sup>15</sup>. The EAG activity thus recorded was then synchronized to a video recording of the moth's flight track (Fig. 2a, b). These moths were tested under conditions identical to those used to measure plume dynamics at  $60\text{ cm s}^{-1}$  with a stationary antenna (Fig. 1b, c). Sampling across 20 individual flights revealed that males encountered odour filaments most frequently in the centre of the plume, with significantly fewer contacts recorded toward the plume edges (Fig. 2c, left). In contrast, the amplitude distribution of in-flight plume contacts was considerably more uniform across the plume (Fig. 2c, right). There was also a marked difference in the mean EAG pulse amplitudes evoked

at rest and in flight, the latter being 2–3 times greater than the former (compare Figs 1c and 2c). These results indicate that the animal's own in-flight movements influence the detection of odour pulses striking the antenna, and that the initial sensory representations of the odour stimulus in the brain may vary considerably depending on the animal's level of activity.

Next, we examined how these rapidly changing spatiotemporal patterns affect the representation of olfactory information in the glomerular circuits in the insect's brain. In male moths, the highly attractive sex-pheromone blend is readily discriminated from deterrent blends released by related species<sup>11–14</sup>. This is accomplished through the selective activation of neurons associated with specific combinations of glomeruli in the male's macroglomerular complex (MGC)<sup>16</sup>. Recordings were made simultaneously from glomerular output neurons (projection neurons; PNs) and the ipsilateral antenna (EAG) in response to point-source odour plumes created inside a small wind tunnel (Fig. 3). Extended recordings from four PNs that responded selectively to only one specific component of the sex-pheromone blend revealed that glomerular output is tightly synchronized to the temporal pattern of peripheral input to the olfactory system (Fig. 3a). Analysis of the variations in instantaneous PN spike frequency as a function of EAG burst amplitude reveals both a progressive increase in the number of spikes evoked as stimulus intensity increases (Fig. 3c) as well as considerable temporal variation in the PN response from trial to trial (Fig. 3b). Closer examination of the temporal structure of PN responses reveals no reproducible pattern of spike timing over dozens of repeated odour presentations (Fig. 4a). Responses vary from regular, tonic firing patterns at low stimulus intensities to more complex phasic-tonic spike trains at higher intensities (Fig. 3a, b). The time interval between maximum EAG amplitude and maximum instantaneous PN frequency also varies as a function of stimulus intensity, from 58.6 ms at low intensities to 14.0 ms at the highest intensities (mean  $\pm$  standard deviation,

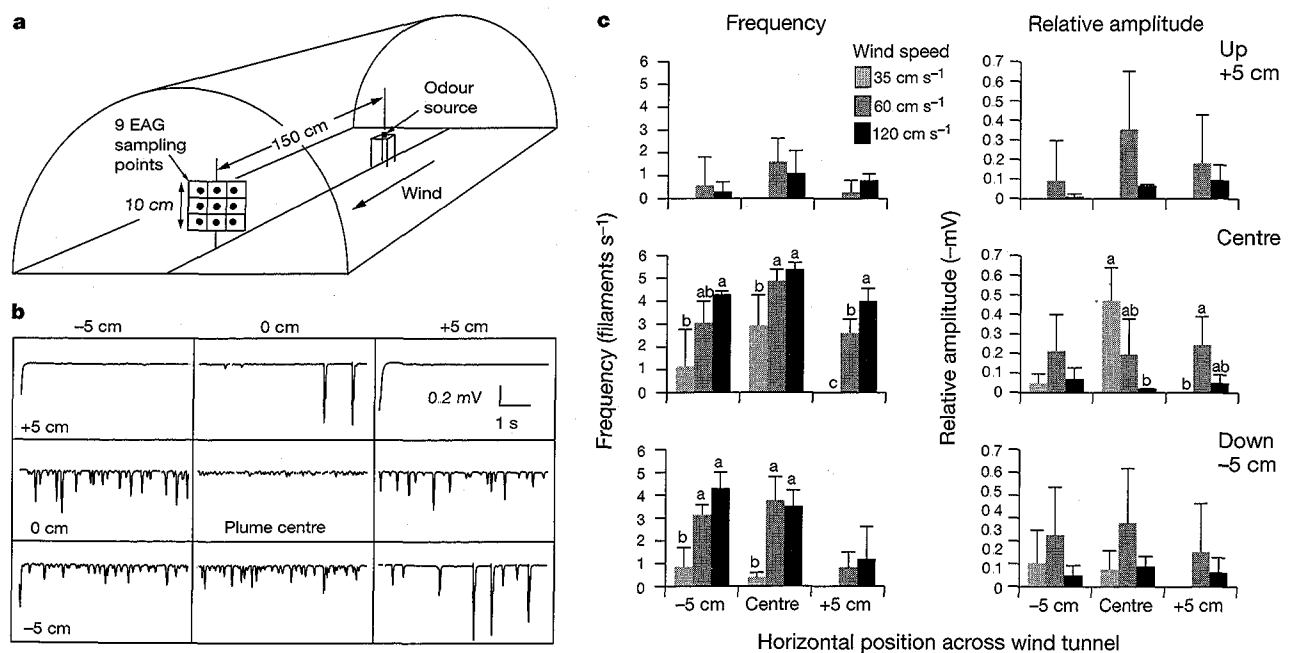


**Figure 1** Mapping the dynamics of a natural odour plume **a**, The electroantennogram (EAG) was used to monitor odour-evoked activity in response to a wind-borne odour plume generated from a point source in a wind tunnel. The positions of the odour source and the nine sequential EAG sampling points 150 cm downwind are indicated. Separation between sampling points was small (5 cm) so that the fine-scale spatiotemporal structure of the plume could be measured. **b**, EAG activity of a single antenna recorded at the nine sampling points, showing position-dependent variation in the amplitude and frequency of

depolarizations (bursts) in response to odour strands over a 5-s period at a wind speed of  $60\text{ cm s}^{-1}$ . **c**, Summary of mean frequency and relative amplitude data illustrating the spatiotemporal dynamics of the odour-evoked EAG activity across the entire nine-point array at different wind speeds ( $n = 3, 5, \text{ and } 2$  for wind speeds of  $35, 60, \text{ and } 120\text{ cm s}^{-1}$ , respectively). Means ( $\pm$  s.d.) at each location were compared across wind speeds (MANOVA, followed by a post-hoc Newman-Keuls test,  $P < 0.05$ )

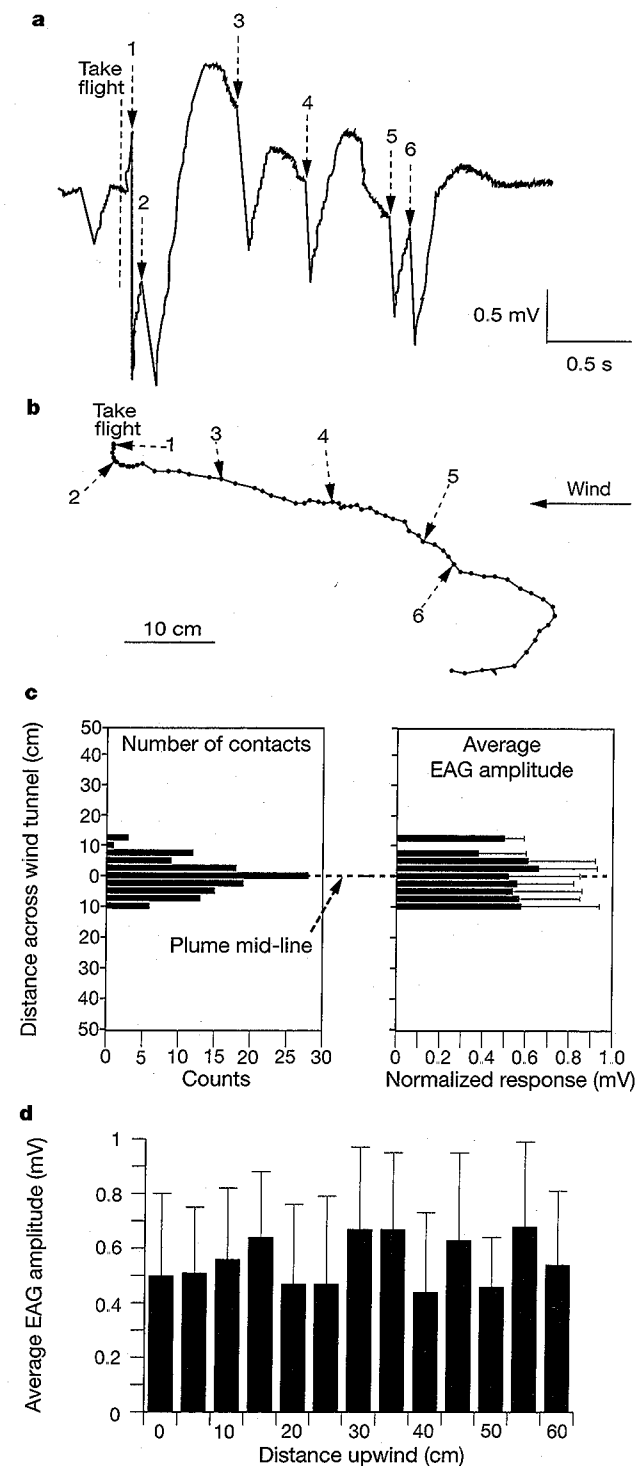


**Figure 2** Measurement of plume dynamics in flight. **a, b**, Simultaneously recorded EAG and flight-track data from an *H. virescens* male. Onsets of EAG bursts are labelled with numbers that correspond to positions of the male along the flight track. Wind direction and the position of the plume midline are indicated by an arrow. We note that all EAG activity recorded during the flight of this male occurred within  $\pm 6$  cm of the plume midline. **c**, Plot of the positions across the wind tunnel (viewed from above) where males encountered pheromone strands, as indicated by bursts of EAG activity. The number of contacts (left) ( $n = 20$  flights) was greatest along the plume midline and decreased rapidly to zero beyond approximately 10 cm to either side of the plume midline, even though flights extended over nearly the entire 1-m width of the wind tunnel. Averaged measurements of EAG relative amplitudes (mean  $\pm$  s.d., right) revealed no significant variation (ANOVA,  $P > 0.5$ ) across the plume. **d**, Normalized EAG amplitudes (mean  $\pm$  s.d.), plotted against their positions along the long axis of the wind tunnel, showed no significant changes with distance from the odour source (ANOVA,  $P > 0.5$ ).

s.d. =  $35.6 \pm 13.3$  ms;  $n = 44$ ). These results were observed whether the PN responded selectively to the major pheromone component ( $n = 2$ ) or to the second essential component ( $n = 2$ ) in the *H. virescens* blend<sup>16</sup>.

Different parameters of the PN response were also shown to be strongly correlated to different time-dependent stimulus features. First, spike-train onset in PNs is closely synchronized to EAG onset, occurring at a nearly constant latency of  $44.3 \pm 1.7$  ms ( $n = 165$ ), regardless of EAG amplitude. Second, both the mean rate and the maximum instantaneous rate of PN spiking are proportional to EAG burst amplitude (Fig. 3c, left), but neither of these parameters varies significantly with its rate of change (EAG onset slope; Fig. 3c, right). Thus, in the moth olfactory system, the time course of PN spike patterns is strongly dependent on both stimulus intensity and plume dynamics.

Synchronous firing among neurons is widely believed to facilitate the integration of related signals in a neural network, thus creating a stronger, more coherent representation of a given stimulus in the brain. In the olfactory system, recent evidence for odour-evoked oscillatory synchronization of PN ensembles has been obtained in several insect species<sup>3-5,9</sup>. Oscillations of brain potentials are also a prominent component of olfactory network activity in moths<sup>7</sup>, and thus we wanted to know whether PNs in the moth antennal lobe are also synchronized by oscillations, or whether synchrony is governed by alternate mechanisms. As a first step, we conducted a temporal analysis of PN responses evoked by many consecutive odour pulses of varying duration and amplitude in a point-source plume (Fig. 4). If PNs were modulated by an evoked wave or network oscillation, PN spike activity would show a strong periodicity in the peristimulus histogram of evoked responses, as shown in other species<sup>3-5,9</sup>. Instead, a histogram of PN instantaneous frequencies (Fig. 4b) revealed non-periodic activity distributed over a very wide frequency range (1.6–185.2 Hz), with little power in the slower frequency range of local field potential (LFP) oscillations (20–50 Hz) reported in moths<sup>7</sup> and other insects<sup>3-5,9</sup>. This finding was confirmed by Fourier analysis (Fig. 4c), which revealed a spectral maximum at only 2.2 Hz, reflecting not the LFP oscillation but the much slower and regular “burst return period” of odour filaments in the plume<sup>10</sup>. Separate studies in the moth *Manduca sexta* have demonstrated that coactivity among PNs is most prominent at response onset, and is neither modulated nor synchronized to any phase of the LFP oscillation (coactivity occurs even in response to brief stimulus pulses which preclude the development of oscillations)<sup>17,18</sup> (see Supplementary Information).

Simultaneous intracellular and EAG recordings indicate, therefore, that the activity of at least some olfactory PNs is time-locked to stimulus dynamics (Figs 3 and 4). Furthermore, the temporal patterning of PN responses is not constrained by an LFP but is highly variable from stimulus to stimulus (Fig. 4). This patterning may be governed in part by an underlying oscillation, but our data indicate that PN response dynamics are more reflective of stimulus dynamics, including changes in stimulus time course and intensity.

The dynamic properties of olfactory stimuli dictate that odour-mediated behaviours must be executed under a wide range of stimulus conditions<sup>10</sup>. For some species, ongoing changes in the environment could have a significant impact on the detection of odour signals by peripheral receptors, and subsequently, on the neural integration of this information in the brain. Behavioural studies have revealed that a patchy olfactory stimulus is more effective than continuous stimulation in sustaining manoeuvres by flying insects to locate the odour source<sup>11-13,19</sup>. In accordance with these studies, our new results provide additional evidence for context-dependent modulation of glomerular output at the very earliest stages of processing in the olfactory system<sup>17</sup>. These findings have implications for deciphering the neural computations used by the brain to discriminate different odours. In other insects, for

example, it was found that different odours activate specific PN assemblies in the antennal lobe, but the patterns of PN spikes are synchronized to a coherent network oscillation<sup>3</sup>. From these studies and others<sup>4,5,9</sup>, it has been suggested that each odour may be uniquely represented by a different temporal pattern of activity across the PN array. Although these findings are intriguing, it remains to be clarified whether such temporal patterns in PN assemblies are maintained under conditions when the spatio-temporal pattern of the stimulus itself is changing rapidly and

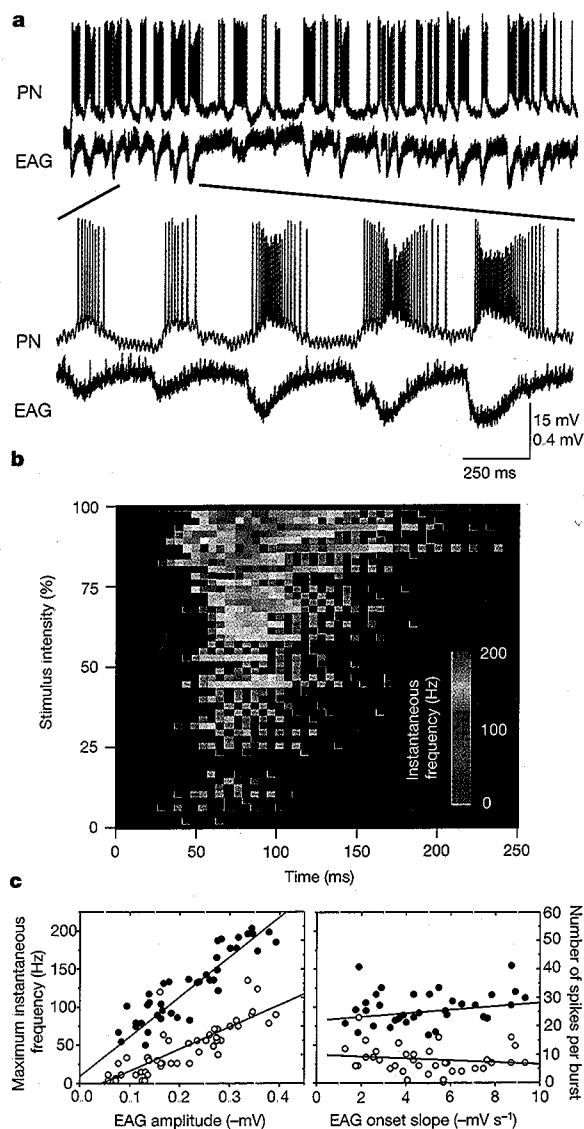


**Figure 3** Temporal patterns of spike discharges in olfactory projection neurons (PNs) are strongly dependent on the stimulus dynamics of a wind-borne pheromone plume **a**, A 15-s segment of activity recorded simultaneously from a PN and the ipsilateral antenna (EAG; upper pair of traces). Detail of the indicated segment is shown in the lower traces (timescale for lower PN-EAG traces only). Throughout the recording, PN activity is tightly correlated with antennal activation **b**, Temporal variations in instantaneous spike frequency as a function of odour intensity (as represented by EAG burst amplitude). Raster plots from each response burst are colour-coded to reflect instantaneous spike frequency. We note that the response patterns become more temporally complex at elevated odour intensities, with increased number and frequency of spikes discharged **c**, Intensity of odour stimulation (left) was tightly correlated to both the maximum instantaneous frequency of PN response (solid circles:  $r^2 = 0.76$ ;  $P < 0.0001$ ) and the number of spikes per odour-evoked burst (open circles:  $r^2 = 0.65$ ;  $P < 0.0001$ ). Other measures of activity such as EAG onset slope (right) did not serve as reliable predictors of central activity.

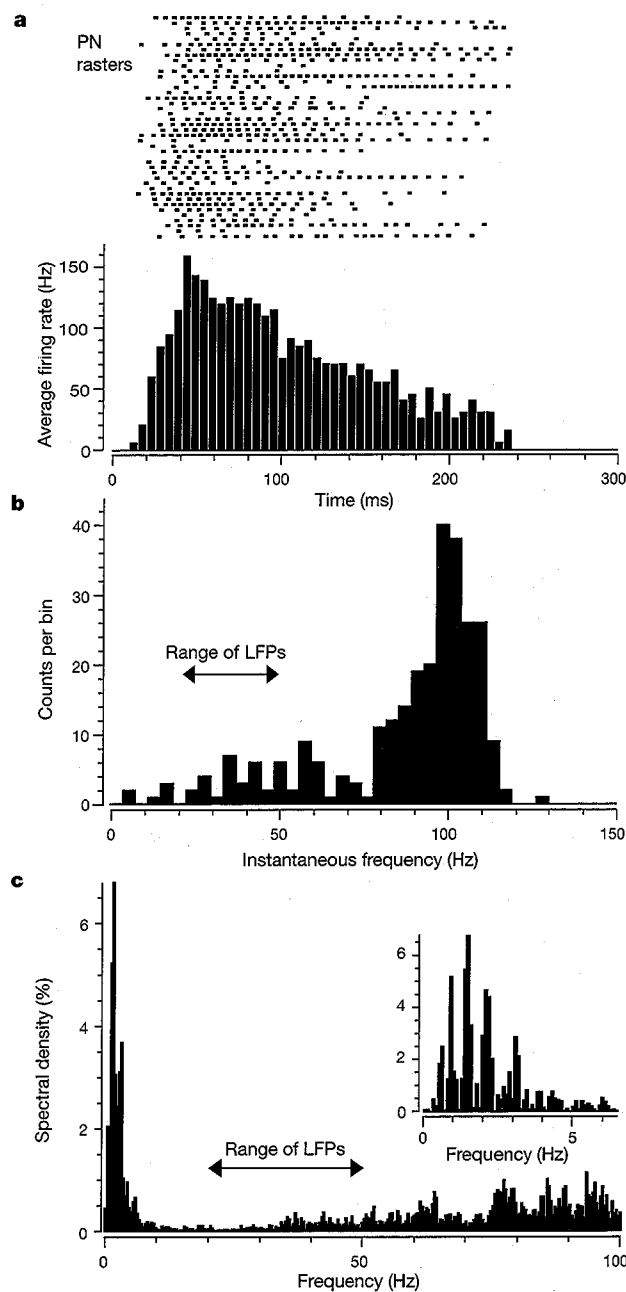


**Figure 4** Temporal analysis of stimulus-evoked PN activity reveals that odour identity is not encoded in the temporal structure of these responses **a**, Sequence of raster plots (upper) from a 20-s recording showing the consecutive responses to 40 odour pulses of varying intensity arising from a point source in the wind tunnel. Time course and number of spikes in each response (3 to 28) were strongly correlated with stimulus intensity, as in Fig. 3a. Summary histogram (lower) shows the average response over time (5-ms bins). Responses are characterized by a rapid rising phase that reaches a single peak in less than 50 ms from onset. This is followed by a slower recovery phase which varies in duration depending on stimulus intensity. The absence of periodicity in spike timing across stimulus intensities further indicates that PN spikes are not tightly synchronized to a slow, repetitive network event like a wave or oscillation. **b**, Instantaneous frequency histogram showing a normal distribution of spike intervals, with a prominent peak near 100 Hz. We note that the great majority of events fall well outside the frequency range of local field potential (LFP) oscillations reported in moths<sup>7</sup> and other insects<sup>3-5,9</sup>. **c**, Spectral analysis of the data revealed the strongest focus of activity below 10 Hz. An expanded plot (inset) shows the spectral peak at 2.2 Hz, reflecting the slow period of spike bursts that characterizes the intermittent response pattern evoked by the fluctuating odour dynamics. The absence of significant peaks in the LFP frequency range again indicates that PN spikes are not significantly entrained to periodic network events such as waves or oscillations.

unpredictably, as occurs in natural odour plumes<sup>10–17</sup>. While our results may be representative of olfactory networks that must monitor the temporal properties of odour plumes, the data show that in the moth antennal lobe, the timing of spike activity across the PN ensemble is not constrained by a periodic network event like an induced wave or oscillation<sup>18</sup>. Instead, timing remains flexible, allowing PN spike trains to be modulated from moment to moment to reflect the changing pattern of olfactory input to the brain. Recent observations in female moths suggest further that these mechanisms are not unique to the male moth's olfactory system or to pheromone-information processing<sup>13,20</sup>. Our new findings therefore support previous studies in both invertebrate and vertebrate sensory systems, arguing that much of the information carried by spikes in sensory systems is associated with stimulus timing<sup>21</sup>. Our new results in moth PNs also support a model of olfactory multitasking in the antennal lobe<sup>22</sup>. We propose that it is through a combination of coding mechanisms that these output neurons are able to report information about both the chemical identity of the stimulus (through their specific spatial association with one or more glomeruli), and the ecologically relevant information about naturally occurring and unpredictable odour dynamics. □

## Methods

### Animals

*Heliothis virescens* (Lepidoptera: Noctuidae) were reared under controlled light (14 h light; 10 h dark), temperature (25–28 °C), and relative humidity (40–60%). All rearing procedures and dissection methods have been described previously<sup>16,21,23</sup>. The procedures used to prepare moths for in-flight EAG measurements have been described elsewhere<sup>15</sup>.

### Flight tunnel

The semicircular wind tunnel used for the stationary and in-flight EAG experiments with *H. virescens* males measured approximately 1 × 1 m in cross-section and 2 m in length. As a stimulus, 10 μl of a 1 mg μl<sup>-1</sup> solution of the species-specific six-component pheromone blend was pipetted onto a rubber septum<sup>15</sup>. The septum was positioned at a height of 15 cm, and a distance of 1.5 m upwind of the stationary EAG preparation (or the take-off platform in the case of the in-flight EAG experiments; see below). Wind speed was varied between 35 cm s<sup>-1</sup> and 120 cm s<sup>-1</sup> for the stationary EAG experiment, and was held constant at 60 cm s<sup>-1</sup> for the in-flight EAG experiments.

### Electrophysiology

Essentially the same EAG preparation was used for both the stationary and in-flight experiments. The exposed and sharpened tips of two Teflon-coated silver wires (100 μm in diameter) were chloridized and inserted into each end of an excised male antenna and then secured with a tiny amount of wax. One wire was attached to the ground, the other connected through a small preamplifier headstage to a Syntech (Hilversum, The Netherlands) d.c. amplifier. For in-flight recordings, the EAG wires were 1.5 m in length, permitting recordings across the entire wind tunnel. For stationary EAG recordings, the preparation was moved through a nine-point sampling grid (Fig. 1a) centred on the plume originating 1.5 m upwind. Each sampling position was monitored for approximately 10 s until the d.c. shift in the trace stabilized<sup>15</sup>. The data reported here were collected for 5 s after trace stabilization.

### Paired EAG/intracellular recordings

Glass micropipettes were used to make recordings from the dendrites of MGC (macroglomerular complex) output neurons<sup>16,23</sup>. Electrodes were filled with 4% Lucifer Yellow CH (Sigma Chemical Company) in 0.2 M LiCl (backfilled with 2 M LiCl) so that neurons could be morphologically identified. Once impaled, each neuron was tested with a standard set of odours and odour mixtures<sup>16,23</sup>. After exposure of the brain and the antennal lobes, the preparation was positioned at the downwind end of another smaller (41 cm inner diameter) wind tunnel especially designed for these experiments. Just before paired EAG/intracellular recording, a rubber septum loaded with pheromone (as above) was placed into the wind tunnel at a distance of 70 cm upwind of the preparation. Wind speed was set at 35 cm s<sup>-1</sup> and the plume created by the point source was allowed to passively stimulate the combined EAG/intracellular recording preparation.

### Analysis

**Stationary EAG.** Frequency and amplitude data were extracted from a 5-s segment of the EAG recordings at each sampling site in the nine-point array (Fig. 1a). Relative EAG amplitudes were calculated to allow quantitative comparison of responses across different antennae. Measurements were taken at three different windspeeds: 35, 60, and 120 cm s<sup>-1</sup>.

**In-flight EAG.** Twenty males were used to obtain in-flight EAG recordings. Each flight track was carefully aligned with respect to pheromone plume position using several fixed markers on the wind tunnel floor. The positions along each track where males encountered a pheromone pulse (as indicated by the simultaneously recorded EAG traces) were marked. From these aligned flight tracks, a composite figure of the positions of EAG bursts for all 20 males was produced. The horizontal cross-section of the wind tunnel was divided into a grid: across-tunnel strips centred on the plume midline were 2.5 cm in width; along-tunnel strips were 5 cm in length. The number of EAG peaks occurring within each across-tunnel strip was then summed and plotted. Relative EAG amplitudes were also calculated and averaged for each across-tunnel (2.5-cm) strip and each along-tunnel (5-cm) strip.

**Paired EAG/intracellular records.** Simultaneous long-term intracellular and EAG recordings were obtained from four preparations, and both records were digitized using Axoscope software (Axon Instruments). Instantaneous frequencies of spike activity were calculated using an in-house algorithm (courtesy of J. K. Douglass). Various response parameters including numbers of spikes per burst, burst durations and intervals, EAG burst amplitudes and onset slopes were measured directly in Axoscope.

Received 7 August 2000; accepted 3 January 2001.

- Adrian, E. D. Olfactory reactions in the brain of the hedgehog. *J. Physiol.* **100**, 459–473 (1942).
- Gelperin, A. & Tank, D. W. Odour-modulated collective network oscillations of olfactory interneurons in a terrestrial mollusc. *Nature* **345**, 437–440 (1990).
- Laurent, G., Wehr, M. & Davidowitz, H. Temporal representations of odors in an olfactory network. *J. Neurosci.* **16**, 3837–3847 (1996).
- Laurent, G. & Davidowitz, H. Encoding of olfactory information with oscillating neural assemblies. *Science* **265**, 1872–1875 (1994).
- Wehr, M. & Laurent, G. Odour encoding by temporal sequences of firing in oscillating neural assemblies. *Nature* **384**, 162–166 (1996).
- Joerges, J., Küttner, A., Galizia, G. & Menzel, R. Representations of odours and odour mixtures visualized in the honeybee brain. *Nature* **387**, 285–288 (1997).
- Heinbockel, T., Kloppenburg, P. & Hildebrand, J. G. Pheromone-evoked potentials and oscillations in the antennal lobes of the sphinx moth *Manduca sexta*. *J. Comp. Physiol. A* **182**, 703–714 (1998).
- Faber, T., Joerges, J. & Menzel, R. Associative learning modifies neural representations of odours in the insect brain. *Nature Neurosci.* **2**, 74–78 (1999).
- Stopfer, M. & Laurent, G. Short-term memory in olfactory network dynamics. *Nature* **402**, 664–668 (1999).
- Murlis, J. in *Insect Pheromone Research: New Directions* (eds Cardé, R. T. & Minks, A. K.) 221–231 (Chapman & Hall, New York, 1997).
- Christensen, T. A., Heinbockel, T. & Hildebrand, J. G. Olfactory information processing in the brain: encoding chemical and temporal features of odors. *J. Neurobiol.* **30**, 82–91 (1996).
- Hildebrand, J. G. Olfactory control of behavior in moths: central processing of odor information and the functional significance of olfactory glomeruli. *J. Comp. Physiol. A* **178**, 5–19 (1996).
- Hansson, B. S. & Christensen, T. A. in *Insect Olfaction* (ed Hansson, B. S.) 125–161 (Springer, Berlin, 1999).
- Christensen, T. A. & White, J. E. in *The Neurobiology of Taste and Smell* Vol. 2 (eds Finger, T. E., Silver, W. I. & Restrepo, D.) 201–232 (Wiley, New York, 2001).
- Vickers, N. J. & Baker, I. C. Reiterative responses to single strands of odor promote sustained upwind flight and odor source location by moths. *Proc. Natl. Acad. Sci. USA* **91**, 5756–5760 (1994).
- Vickers, N. J., Christensen, T. A. & Hildebrand, J. G. Combinatorial odor discrimination in the brain: attractive and antagonist odor blends are represented in distinct combinations of uniquely identifiable glomeruli. *J. Comp. Neurol.* **400**, 35–56 (1998).
- Christensen, T. A., Pawlowski, V. M., Lei, H. & Hildebrand, J. G. Multi-unit recordings reveal context-dependent modulation of synchrony in odor-specific neural ensembles. *Nature Neurosci.* **3**, 927–931 (2000).
- Lei, H., Christensen, T. A. & Hildebrand, J. G. Odor-evoked synchronization of olfactory networks: comparison of output neurons innervating the same and different glomeruli in the antennal lobe of *Manduca sexta*. *Soc. Neurosci. Abstr.* **26**, 1208 (2000).
- Baker, I. C. & Vickers, N. J. in *Insect Pheromone Research: New Directions* (eds Cardé, R. T. & Minks, A. K.) 248–264 (Chapman & Hall, New York, 1997).
- King, J. R., Christensen, T. A. & Hildebrand, J. G. Response characteristics of an identified, sexually dimorphic olfactory glomerulus. *J. Neurosci.* **20**, 2391–2399 (2000).
- Buračas, G. I. & Albright, T. D. Gauging sensory representations in the brain. *Trends Neurosci.* **22**, 303–309 (1999).
- Christensen, T. A., Waldrop, B. R. & Hildebrand, J. G. Multitasking in the olfactory system: context dependent responses to odors reveal dual GABA-regulated coding mechanisms in single olfactory projection neurons. *J. Neurosci.* **18**, 5999–6008 (1998).
- Christensen, T. A., Mustaparta, H. & Hildebrand, J. G. Chemical communication in heliothine moths VI. Parallel pathways for information processing in the macroglomerular complex of the male tobacco budworm moth *Heliothis virescens*. *J. Comp. Physiol. A* **177**, 545–557 (1995).

Supplementary information is available on Nature's World-Wide Web site (<http://www.nature.com>) or as paper copy from the London editorial office of Nature.

### Acknowledgements

We thank S. Hannaford and M. Willis for help in constructing the small wind tunnel. This work was supported by United States Department of Agriculture (National Research Initiative), National Institutes of Health (National Institute for Deafness and Other Communication Disorders), and Defense Advanced Research Projects Agency (Controlled Biological Systems).

Correspondence and requests for materials should be addressed to N.J.V. (e-mail: [vickers@biology.utah.edu](mailto:vickers@biology.utah.edu)).